

A SPECTRAL LOD METHOD FOR MULTISCALE PROBLEMS WITH HIGH CONTRAST

SUSANNE C. BRENNER, JOSÉ C. GARAY, AND LI-YENG SUNG

ABSTRACT. We present a multiscale finite element method for a diffusion problem with rough and high contrast coefficients. The construction of the multiscale finite element space is based on the localized orthogonal decomposition methodology and it involves solutions of local finite element eigenvalue problems. We show that the performance of the multiscale finite element method is similar to the performance of standard finite element methods for the homogeneous Dirichlet boundary value problem for the Poisson equation on smooth or convex domains. Simple explicit error estimates are established under conditions that can be verified from the outputs of the computation.

1. INTRODUCTION

Let Ω be the unit square $(0, 1) \times (0, 1)$. We consider the following model problem: Find $u \in H_0^1(\Omega)$ such that

$$(1.1) \quad a(u, v) = \int_{\Omega} fv \, dx \quad \forall v \in H_0^1(\Omega),$$

where

$$a(u, v) = \int_{\Omega} \kappa \nabla u \cdot \nabla v \, dx,$$

and the diffusion coefficient $\kappa(x) \in L^{\infty}(\Omega)$ is a piecewise constant function such that $\min_{x \in \Omega} \kappa(x) = 1$ and $\max_{x \in \Omega} \kappa(x) = \beta$.

Remark 1.1. We follow the standard notation for function spaces and norms that can be found for example in [1].

Accordingly, we have

$$(1.2) \quad |v|_{H^1(\Omega)} \leq \|v\|_a \quad \forall v \in H^1(\Omega),$$

where $\|v\|_a = \sqrt{a(v, v)}$ is the energy norm.

Let \mathcal{T}_H be a uniform coarse triangulation of Ω with m (closed) elements K_1, \dots, K_m (cf. Figure 1.1 (left)), where H is the length of the edges of the squares in \mathcal{T}_H . The Q_1 finite element subspace of $H_0^1(\Omega)$ associated with \mathcal{T}_H (cf. [6, 4]) is denoted by V_H .

Date: November 1, 2025.

2020 Mathematics Subject Classification. 65N30, 65N15.

Key words and phrases. multiscale diffusion problem, rough coefficient, high contrast, spectral coarse space, LOD .

This work was supported in part by the National Science Foundation under Grant No. DMS-22-08404 and Grant No. DMS-25-13273.

| K_1 | K_2 | K_3 | K_4 |
|----------|----------|----------|----------|
| K_5 | K_6 | K_7 | K_8 |
| K_9 | K_{10} | K_{11} | K_{12} |
| K_{13} | K_{14} | K_{15} | K_{16} |

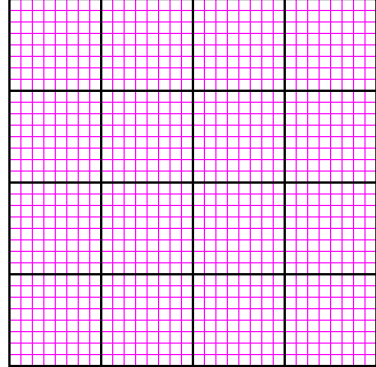


FIGURE 1.1. A coarse mesh \mathcal{T}_H with 16 elements (left) and a fine mesh \mathcal{T}_h (right).

Let \mathcal{T}_h be a fine triangulation of Ω obtained by a uniform refinement of \mathcal{T}_H (cf. Figure 1.1 (right)). The Q_1 finite element subspace of $H_0^1(\Omega)$ associated with \mathcal{T}_h is denoted by V_h . We use \mathcal{V}_h to denote the set of interior vertices of \mathcal{T}_h .

Let $u_h \in V_h$ be the standard finite element solution of (1.1), i.e.,

$$(1.3) \quad a(u_h, v) = \int_{\Omega} f v \, dx \quad \forall v \in V_h.$$

Remark 1.2. We have a Poincaré-Friedrichs inequality

$$(1.4) \quad \|v\|_{L^2(\Omega)} \leq |v|_{H^1(\Omega)} \quad \forall v \in H_0^1(\Omega)$$

on the unit square Ω , which together with (1.2) and (1.3) implies that

$$(1.5) \quad \|u_h\|_a \leq \|f\|_{L^2(\Omega)}.$$

We assume u_h is a good approximation of u , which means in particular that $\kappa(x)$ should be resolved by \mathcal{T}_h . However the computation of u_h is expensive because $\dim V_h \gg 1$, especially if we have to solve for different f 's repeatedly. On the other hand the standard finite element solution $u_H \in V_H$, while affordable because $\dim V_H \ll \dim V_h$, is a poor approximation of u . Therefore we need to design a multiscale finite element method that bridges the two scales.

We will construct the multiscale finite element method through the localized orthogonal decomposition strategy (cf. [11, 15, 16]) and by using a coarse space consisting of local eigenfunctions.

There is a substantial literature on solving multiscale problems by using local eigenfunctions (cf. [7, 8, 2, 23, 12, 5, 17, 13, 14, 18]). Our approach is related to the work in [5]. The global multiscale finite element spaces in [5] and this paper are identical, albeit their bases are generated differently. On the other hand, the localized multiscale finite element spaces are different. Instead of solving a local version of the global problem as in [5], we construct our multiscale finite element space $V_{aux,k}^{\text{ms},h}$ by solving the corrector equation through k iterations of a preconditioned conjugate gradient algorithm. Our main theoretical result is an estimate of the form

$$\|u_h - u_{aux,k}^{\text{ms},h}\|_a \leq C_{\dagger} H \|f\|_{L^2(\Omega)},$$

provided that $k \geq k_{\dagger}$. Here $u_{aux,k}^{ms,h}$ is the Galerkin solution of (1.1) for the space $V_{aux,k}^{ms,h}$ and the explicit constants C_{\dagger} and k_{\dagger} are calculated from the outputs of the computation in the construction of $V_{aux,k}^{ms,h}$. Thus the construction and analysis of our method for (1.1) is *a posteriori* in nature. In particular the analysis does not require the exponential decay of the basis functions of the multiscale finite element space.

The rest of the paper is organized as follows. We introduce the auxiliary space V_{aux} comprised of local eigenfunctions in Section 2, and construct in Section 3 an operator Π_{aux} from V_h to V_{aux} that has a desired approximation property. The ideal (or global) multiscale finite element method is analyzed in Section 4, followed by the construction of a localized multiscale finite element method in Section 5. The analysis of the localized multiscale method is carried out in Section 6 and corroborating numerical results are presented in Section 7. We end the paper with some concluding remarks in Section 8. Appendix A provides some eigenvalue estimates that are used in the computation.

2. THE AUXILIARY SPACE V_{aux}

On each element $K_i \in \mathcal{T}_H$, we construct the local auxiliary space $V_{aux}^{(i)}$ by solving an eigenvalue problem.

Let $V_h(K_i)$ be the restriction of V_h to K_i and $n_i = \dim V_h(K_i)$. Note that $v \in V_h(K_i)$ vanishes on $\partial K_i \cap \partial\Omega$. We will denote by $\overset{\circ}{V}_h(K_i)$ the subspace of $V_h(K_i)$ whose members vanish on ∂K_i .

According to the finite dimensional Spectral Theorem (cf. [10, Section 79]), there exist eigenvalues $0 \leq \lambda_1^{(i)} \leq \dots \leq \lambda_{n_i}^{(i)}$ and corresponding eigenfunctions $\psi_1^{(i)}, \dots, \psi_{n_i}^{(i)}$ such that

$$(2.1) \quad \int_{K_i} \kappa \nabla \psi_j^{(i)} \cdot \nabla w \, dx = \lambda_j^{(i)} H^{-2} \int_{K_i} \kappa \psi_j^{(i)} w \, dx \quad \forall w \in V_h(K_i),$$

$$(2.2) \quad H^{-2} \int_{K_i} \kappa (\psi_j^{(i)})^2 \, dx = 1.$$

We can rewrite (2.1) and (2.2) concisely as

$$a_i(\psi_j^{(i)}, w) = \lambda_j^{(i)} s_i(\psi_j^{(i)}, w) \quad \forall w \in V_h(K_i) \quad \text{and} \quad s_i(\psi_j^{(i)}, \psi_j^{(i)}) = 1,$$

where

$$\begin{aligned} a_i(v, w) &= \int_{K_i} \kappa \nabla v \cdot \nabla w \, dx \quad \forall v, w \in V_h(K_i), \\ s_i(v, w) &= H^{-2} \int_{K_i} \kappa v w \, dx \quad \forall v, w \in V_h(K_i). \end{aligned}$$

The functions $\psi_j^{(i)}$ for $1 \leq j \leq n_i$ form an orthonormal basis of the inner product space $(V_h(K_i), s_i(\cdot, \cdot))$. Given any $v \in V_h(K_i)$, we can write

$$(2.3) \quad v = \sum_{j=1}^{n_i} c_j \psi_j^{(i)}$$

and then we have

$$(2.4) \quad \|v\|_{L^2(K_i; \kappa)}^2 = \int_{K_i} \kappa v^2 dx = H^2 \sum_{j=1}^{n_i} c_j^2,$$

$$(2.5) \quad \|v\|_{a_i}^2 = \int_{K_i} \kappa |\nabla v|^2 dx = \sum_{j=1}^{n_i} \lambda_j^{(i)} c_j^2.$$

We define

$$(2.6) \quad V_{aux}^{(i)} = \text{span}\{\psi_1^{(i)}, \dots, \psi_{L_i}^{(i)}\},$$

where L_i is sufficiently large so that

$$(2.7) \quad \lambda_j^{(i)} > \frac{1}{2} \mu_i \quad \text{if } j > L_i,$$

and μ_i is the first nonzero eigenvalue of the analog of (2.1)–(2.2) for the Laplace operator (i.e., $\kappa = 1$) on K_i .

Remark 2.1. Due to the scaling factor H^{-2} in (2.1), the eigenvalue μ_i in (2.7) is ≈ 1 . Moreover it can be shown (cf. Appendix A) that

$$\begin{aligned} \mu_i &> \pi^2 && \text{if } K_i \text{ is disjoint from } \partial\Omega, \\ \mu_i &> \pi^2/4 && \text{if only one of the edges of } K_i \text{ is on } \partial\Omega, \\ \mu_i &> \pi^2/2 && \text{if two of the edges of } K_i \text{ are on } \partial\Omega. \end{aligned}$$

Remark 2.2. L_i is bounded by the number of high contrast channels or inclusions in K_i (cf. [8, Appendix A]).

Remark 2.3. The cost for computing $\psi_1^{(i)}, \dots, \psi_{L_i}^{(i)}$ is $O((n/m)^3)$, where $n = \dim V_h$, and the eigenfunctions associated with different elements of \mathcal{T}_H can be computed in parallel.

The global auxiliary space

$$V_{aux} = V_{aux}^{(1)} \oplus \dots \oplus V_{aux}^{(m)}$$

is the direct sum of the local auxiliary spaces, and

$$(2.8) \quad \dim V_{aux} = \sum_{i=1}^m \dim V_{aux}^{(i)} = \sum_{i=1}^m L_i \stackrel{\text{def}}{=} L.$$

3. THE OPERATOR Π_{aux}

Let $v = \sum_{j=1}^{n_i} c_j \psi_j^{(i)}$ be an arbitrary function in $V_h(K_i)$. The local projection operator $\Pi_{aux}^{(i)} : V_h(K_i) \rightarrow V_{aux}^{(i)}$ is defined by

$$(3.1) \quad \Pi_{aux}^{(i)} v = \sum_{j=1}^{L_i} c_j \psi_j^{(i)} = \sum_{j=1}^{L_i} s_i(v, \psi_j^{(i)}) \psi_j^{(i)},$$

i.e., $\Pi_{aux}^{(i)}$ is the orthogonal projection operator associated with the inner product $s_i(\cdot, \cdot)$.

It follows from (2.3), (2.5) and (3.1) that

$$(3.2) \quad \|\Pi_{aux}^{(i)} v\|_{a_i}^2 = \sum_{1 \leq j \leq L_i} \lambda_j^{(i)} c_j^2 \leq \sum_{1 \leq j \leq n_i} \lambda_j^{(i)} c_j^2 = \|v\|_{a_i}^2,$$

and in view of (2.4), (2.5), (2.7) and Remark 2.1,

$$(3.3) \quad \begin{aligned} H^{-2} \|v - \Pi_{aux}^{(i)} v\|_{L^2(K_i; \kappa)}^2 &= \sum_{L_i < j \leq n_i} c_j^2 \\ &\leq \sum_{L_i < j \leq n_i} [\lambda_j^{(i)}]^{-1} \lambda_j^{(i)} c_j^2 \leq \frac{2}{\mu_i} \sum_{L_i < j \leq n_i} \lambda_j^{(i)} c_j^2 \leq C_*^2 \|v\|_{a_i}^2, \end{aligned}$$

where (cf. Remark 2.1)

$$(3.4) \quad C_* = 2^{3/2} \pi \geq \left(2 \max_{1 \leq i \leq m} (1/\mu_i) \right)^{\frac{1}{2}}.$$

Let

$$\tilde{V}_h = V_h(K_1) \oplus \cdots \oplus V_h(K_m)$$

be the direct sum of $V_h(K_i)$. The projection operator $\Pi_{aux} : \tilde{V}_h \longrightarrow V_{aux} (\subset \tilde{V}_h)$ is given by

$$(\Pi_{aux} \tilde{v})_i = \Pi_{aux}^{(i)} v_i,$$

where $\tilde{v} = (v_1, \dots, v_m) \in \tilde{V}_h$ (with $v_i \in V_h(K_i)$).

For a function $\tilde{v} \in \tilde{V}_h$, we define

$$(3.5) \quad \|\tilde{v}\|_{L^2(\Omega; \kappa)} = \left(\sum_{i=1}^m \int_{K_i} \kappa v_i^2 dx \right)^{\frac{1}{2}} = \left(\sum_{i=1}^m \|v_i\|_{L^2(K_i; \kappa)}^2 \right)^{\frac{1}{2}},$$

$$(3.6) \quad \|\tilde{v}\|_a = \left(\sum_{i=1}^m \int_{K_i} \kappa |\nabla v_i|^2 dx \right)^{\frac{1}{2}} = \left(\sum_{i=1}^m \|v_i\|_{a_i}^2 \right)^{\frac{1}{2}}.$$

The following result is an immediate consequence of the local estimates (3.2), (3.3) and the definitions (3.5) and (3.6).

Lemma 3.1. *We have*

$$\|\Pi_{aux} \tilde{v}\|_a \leq \|\tilde{v}\|_a \quad \forall \tilde{v} \in \tilde{V}_h$$

and

$$\|\tilde{v} - \Pi_{aux} \tilde{v}\|_{L^2(\Omega; \kappa)} \leq C_* H \|\tilde{v}\|_a \quad \forall \tilde{v} \in \tilde{V}_h.$$

Remark 3.2. We can identify $v \in V_h$ with $\tilde{v} = (v_1, \dots, v_m) \in \tilde{V}_h$, where $v_i = v|_{K_i}$ is the restriction of v on K_i , and we have

$$\|\tilde{v}\|_{L^2(\Omega; \kappa)} = \left(\int_{\Omega} \kappa v^2 dx \right)^{\frac{1}{2}} = \|v\|_{L^2(\Omega; \kappa)} \quad \text{and} \quad \|\tilde{v}\|_a = \left(\int_{\Omega} \kappa |\nabla v|^2 dx \right)^{\frac{1}{2}} = \|v\|_a.$$

According to Remark 3.2, we can identify V_h with a subspace of \tilde{V}_h . Hence Π_{aux} is defined on V_h , and

$$(3.7) \quad \Pi_{aux} v = (\Pi_{aux}^{(i)}(v|_{K_1}), \dots, \Pi_{aux}^{(m)}(v|_{K_m})) \quad \forall v \in V_h.$$

But the restriction of Π_{aux} to V_h , still denoted by Π_{aux} , is no longer a projection because $V_{aux} \subset \tilde{V}_h$ is not a subspace of $V_h \subset \tilde{V}_h$.

Remark 3.3. The idea of using a nonconforming coarse subspace in the construction of a localized orthogonal decomposition method was also employed in [19].

We will use $\text{Ker } \Pi_{aux}$ to represent the kernel of Π_{aux} in V_h , i.e.,

$$(3.8) \quad \text{Ker } \Pi_{aux} = \{v \in V_h : \Pi_{aux}v = 0\} = \{v \in V_h : \Pi_{aux}^{(i)}(v|_{K_i}) = 0 \text{ for } 1 \leq i \leq m\}.$$

The functions in $\text{Ker } \Pi_{aux}$ satisfy an important estimate that follows from Lemma 3.1 and Remark 3.2:

$$(3.9) \quad \|w\|_{L^2(\Omega; \kappa)} = \|w - \Pi_{aux}w\|_{L^2(\Omega; \kappa)} \leq C_* H \|w\|_a \quad \forall w \in \text{Ker } \Pi_{aux}.$$

4. THE IDEAL (OR GLOBAL) MULTISCALE FINITE ELEMENT METHOD

The ideal (or global) multiscale finite element space $V_{aux}^{\text{ms},h}$ is the subspace of V_h orthogonal to $\text{Ker } \Pi_{aux}$ with respect to the bilinear form $a(\cdot, \cdot)$, i.e.,

$$(4.1) \quad V_{aux}^{\text{ms},h} = \{v \in V_h : a(v, w) = 0 \quad \forall w \in \text{Ker } \Pi_{aux}\}.$$

It follows that

$$(4.2) \quad \dim V_{aux}^{\text{ms},h} = \dim V_h - \dim \text{Ker } \Pi_{aux}.$$

The ideal multiscale finite element method is to find $u_{aux}^{\text{ms},h} \in V_{aux}^{\text{ms},h}$ defined by

$$(4.3) \quad a(u_{aux}^{\text{ms},h}, v) = \int_{\Omega} fv \, dx \quad \forall v \in V_{aux}^{\text{ms},h}.$$

There is a simple error analysis for the ideal multiscale finite element method.

Theorem 4.1. *Let $u_h \in V_h$ be the solution of (1.3). We have*

$$(4.4) \quad \|u_h - u_{aux}^{\text{ms},h}\|_a \leq C_* H \|\kappa^{-1/2} f\|_{L^2(\Omega)} \leq C_* H \|f\|_{L^2(\Omega)},$$

where C_* is the positive constant defined by (3.4).

Proof. From (4.1) and the Galerkin orthogonality

$$a(u_h - u_{aux}^{\text{ms},h}, w) = 0 \quad \forall w \in V_{aux}^{\text{ms},h}$$

that follows from (1.1) and (4.3), we see that $u_h - u_{aux}^{\text{ms},h} \in \text{Ker } \Pi_{aux}$.

Therefore we have, by (1.1), (3.9), (4.1) and the Cauchy-Schwarz inequality,

$$\begin{aligned} \|u_h - u_{aux}^{\text{ms},h}\|_a^2 &= a(u_h - u_{aux}^{\text{ms},h}, u_h - u_{aux}^{\text{ms},h}) \\ &= a(u_h, u - u_{aux}^{\text{ms},h}) \\ &= \int_{\Omega} f(u_h - u_{aux}^{\text{ms},h}) \, dx \\ &\leq \|\kappa^{-1/2} f\|_{L^2(\Omega)} \|u_h - u_{aux}^{\text{ms},h}\|_{L^2(\Omega; \kappa)} \\ &\leq \|\kappa^{-1/2} f\|_{L^2(\Omega)} C_* H \|u_h - u_{aux}^{\text{ms},h}\|_a, \end{aligned}$$

which implies (4.4). \square

It follows from Theorem 4.1 and a standard duality argument that

$$(4.5) \quad \|u_h - u_{aux}^{\text{ms},h}\|_{L^2(\Omega; \kappa)} \leq (C_* H)^2 \|\kappa^{-1/2} f\|_{L^2(\Omega)} \leq (C_* H)^2 \|f\|_{L^2(\Omega)}.$$

4.1. A Basis for $\text{Ker } \Pi_{aux}$. In order to construct a basis for $V_{aux}^{\text{ms},h}$, first we need a basis for $\text{Ker } \Pi_{aux}$.

Assumption Given K_i , we can find L_i nodes $\hat{p}_1^{(i)}, \dots, \hat{p}_{L_i}^{(i)}$ of \mathcal{T}_h in the interior of K_i (cf. Figure 4.1 where $L_i = 3$) such that the matrix S_i defined by

$$S_i(j, k) = s_i(\hat{\phi}_j^{(i)}, \psi_k^{(i)}) \quad 1 \leq j, k \leq L_i$$

is nonsingular, where $\hat{\phi}_j^{(i)}$ is the hat function (from V_h) associated with the node \hat{p}_j normalized so that

$$(4.6) \quad a_i(\hat{\phi}_j^{(i)}, \hat{\phi}_j^{(i)}) = 1.$$

We will refer to these nodes as the dual nodes and denote by V_h^d the space spanned by the functions $\hat{\phi}_j^{(i)}$ for $1 \leq i \leq m$ and $1 \leq j \leq L_i$. In view of (2.8), we have

$$(4.7) \quad \dim V_h^d = L = \dim V_{aux}.$$

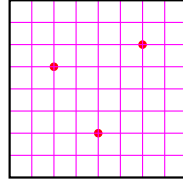


FIGURE 4.1. The dual nodes $\hat{p}_1^{(i)}, \hat{p}_2^{(i)}$ and $\hat{p}_3^{(i)}$ in K_i represented by the red dots, where $L_i = 3$.

Remark 4.2. As h goes to zero, the eigenfunctions $\psi_j^{(i)}$ ($1 \leq j \leq L_i$) approach the eigenfunctions of the corresponding continuous eigenproblem posed on the subspace of $H^1(K_i)$ whose members vanish on $\partial K_i \cap \partial \Omega$, and hence they can be approximated accurately in the norm of $L^2(K_i; \kappa)$ by functions in $\mathring{V}_h(K_i)$. Consequently, for h sufficiently small, there exist functions $\zeta_1, \dots, \zeta_{L_i} \in \mathring{V}_h(K_i)$ such that the matrix \mathcal{S}_i defined by

$$\mathcal{S}_i(j, k) = s_i(\zeta_j, \psi_k^{(i)}) \quad 1 \leq j, k \leq L_i$$

is nonsingular. This means the rank of the matrix with components $s_i(\phi_\ell^{(i)}, \psi_k^{(i)})$ for $1 \leq \ell \leq \tilde{n}_i$ and $1 \leq k \leq L_i$ is L_i , where $\tilde{n}_i = \dim \mathring{V}_h(K_i)$ and $\phi_\ell^{(i)}$ ($1 \leq \ell \leq \tilde{n}_i$) is the normalized hat function associated with the node p_ℓ interior to K_i . Therefore the existence of dual nodes is guaranteed. Moreover in this case it is also very likely that a set of L_i randomly chosen interior nodes of K_i can be used as dual nodes.

Remark 4.3. In practice we just choose the dual nodes $\hat{p}_1, \dots, \hat{p}_{L_i}$ randomly and verify that the matrix S_i is nonsingular. It is also convenient for the error analysis that the dual nodes are chosen to be separated, i.e., any element of \mathcal{T}_h can have at most one of the dual nodes as a vertex (cf. Figure 4.1). Consequently we have

$$(4.8) \quad a(\hat{\phi}_j^{(i)}, \hat{\phi}_{j'}^{(i')}) = \begin{cases} 1 & \text{if } i = i' \text{ and } j = j' \\ 0 & \text{otherwise} \end{cases}.$$

Observe that the existence of dual nodes in K_i implies that $\Pi_{aux}^{(i)} : \mathring{V}_h(K_i) \longrightarrow V_{aux}^{(i)}$ is a surjection. It follows that $\Pi_{aux} : V_h \longrightarrow V_{aux}$ is also a surjection and hence (cf. (2.8))

$$(4.9) \quad \dim \text{Ker } \Pi_{aux} = \dim V_h - \dim V_{aux} = \dim V_h - L,$$

which together with (4.2) implies that

$$(4.10) \quad \dim V_{aux}^{\text{ms},h} = L.$$

Let the functions $\tilde{\phi}_1^{(i)}, \dots, \tilde{\phi}_{L_i}^{(i)}$ in $\text{span}\{\hat{\phi}_1^{(i)}, \dots, \hat{\phi}_{L_i}^{(i)}\}$ satisfy

$$(4.11) \quad s_i(\tilde{\phi}_j^{(i)}, \psi_k^{(i)}) = \delta_{jk} = \begin{cases} 1 & \text{if } j = k \\ 0 & \text{if } j \neq k \end{cases}.$$

These dual functions are given by

$$\tilde{\phi}_j^{(i)} = \sum_{\ell=1}^{L_i} \tau_{j\ell}^{(i)} \hat{\phi}_{\ell}^{(i)} \quad \text{for } 1 \leq j \leq L_i,$$

where $\tau_{j\ell}^{(i)}$ are the components of the matrix S_i^{-1} . Note that

$$(4.12) \quad \text{span}\{\tilde{\phi}_1^{(i)}, \dots, \tilde{\phi}_{L_i}^{(i)}\} = \text{span}\{\hat{\phi}_1^{(i)}, \dots, \hat{\phi}_{L_i}^{(i)}\}.$$

We define the number

$$(4.13) \quad M_i = \text{the 2-norm of the } L_i \times L_i \text{ matrix with components } a(\tilde{\phi}_j^{(i)}, \tilde{\phi}_{\ell}^{(i)}).$$

It will play a role in the error analysis in Section 6.

Remark 4.4. It follows from (3.1) and (4.11) that

$$(4.14) \quad \Pi_{aux}^{(i)} \tilde{\phi}_j^{(i)} = \psi_j^{(i)} \quad \text{for } 1 \leq j \leq L_i.$$

Consequently $\Pi_{aux} : V_h^d \longrightarrow V_{aux}$ is an isomorphism by (2.8), (4.7) and (4.12).

Let $\mathcal{N}_{aux} = \{\hat{p}_j^{(i)} : 1 \leq i \leq m, 1 \leq j \leq L_i\}$ be the set of the dual nodes in \mathcal{T}_h . Given any node $p \in \mathcal{V}_h \setminus \mathcal{N}_{aux}$, denote by ϕ_p the hat function (in V_h) associated with p normalized by $\|\phi_p\|_a = 1$. Let the function $\tilde{\phi}_p \in V_h$ be defined by

$$(4.15) \quad \tilde{\phi}_p = \sum_{i=1}^m \sum_{j=1}^{L_i} s_i(\phi_p, \psi_j^{(i)}) \tilde{\phi}_j^{(i)}.$$

Lemma 4.5. *The function $\phi_p - \tilde{\phi}_p$ belongs to $\text{Ker } \Pi_{aux}$ and $\{\phi_p - \tilde{\phi}_p : p \in \mathcal{V}_h \setminus \mathcal{N}_{aux}\}$ is a basis of $\text{Ker } \Pi_{aux}$.*

Proof. It follows from (3.1), (4.14) and (4.15) that

$$\Pi_{aux}^{(i)} \phi_p = \sum_{j=1}^{L_j} s_i(\phi_p, \psi_j^{(i)}) \psi_j^{(i)} = \Pi_{aux}^{(i)} \tilde{\phi}_p \quad \text{for } 1 \leq i \leq m$$

and hence $\phi_p - \tilde{\phi}_p$ belongs to $\text{Ker } \Pi_{aux}$ defined in (3.8).

Since the functions $\phi_p - \tilde{\phi}_p$ satisfy the Kronecker property

$$(\phi_p - \tilde{\phi}_p)(p') = \begin{cases} 1 & \text{if } p = p' \\ 0 & \text{if } p \neq p' \end{cases} \quad \text{for } p, p' \in \mathcal{V}_h \setminus \mathcal{N}_{aux},$$

they are linearly independent and the total number of these functions is precisely $\dim V_h - L = \dim \text{Ker } \Pi_{aux}$ by (4.9). \square

Remark 4.6. The function $\tilde{\phi}_p$ is supported (i) on one element of \mathcal{T}_h if p is interior to the element, (ii) on two elements of \mathcal{T}_h if p is in the interior of the common edge of the two elements, or (iii) on four elements of \mathcal{T}_h if p is the common vertex of these elements. These three possibilities are illustrated by the blue dots in Figure 4.2.

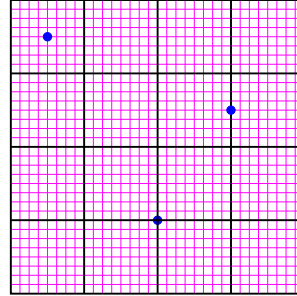


FIGURE 4.2. The three possibilities for $p \in \mathcal{V}_h \setminus \mathcal{N}_{aux}$

4.2. A Basis for $V_{aux}^{\text{ms},h}$. We are now ready to construct a basis of $V_{aux}^{\text{ms},h}$. Let the projection $\mathfrak{C}_h : V_h \longrightarrow \text{Ker } \Pi_{aux}$ be defined by

$$(4.16) \quad a(\mathfrak{C}_h v, w) = a(v, w) \quad \forall w \in \text{Ker } \Pi_{aux}.$$

Remark 4.7. Comparing (1.3), (4.1), (4.3) and (4.16), we see that

$$(4.17) \quad u_h - u_{aux}^{\text{ms},h} = \mathfrak{C}_h u_h.$$

We can use the normalized hat functions associated with the dual nodes (cf. Section 4.1) and the correction operator \mathfrak{C}_h to construct a basis for $V_{aux}^{\text{ms},h}$.

Lemma 4.8. *The set $\{\hat{\phi}_j^{(i)} - \mathfrak{C}_h \hat{\phi}_j^{(i)} : 1 \leq i \leq m, 1 \leq j \leq L_i\}$ is a basis of $V_{aux}^{\text{ms},h}$, where $\hat{\phi}_j^{(i)}$ is the normalized hat function corresponding to a dual node $\hat{p}_j^{(i)}$ in the interior of K_i .*

Proof. It follows from (4.16) that $\hat{\phi}_j^{(i)} - \mathfrak{C}_h \hat{\phi}_j^{(i)}$ belongs to $V_{aux}^{\text{ms},h}$ defined by (4.1).

Note that the functions in $\{\hat{\phi}_j^{(i)} - \mathfrak{C}_h \hat{\phi}_j^{(i)} : 1 \leq i \leq m, 1 \leq j \leq L_i\}$ are linearly independent because we have the relations (cf. (4.12) and (4.14))

$$\begin{aligned} & \text{span}\{\Pi_{aux}^{(i)}(\hat{\phi}_j^{(i)} - \mathfrak{C}_h \hat{\phi}_j^{(i)}) : 1 \leq i \leq m, 1 \leq j \leq L_i\} \\ &= \text{span}\{\Pi_{aux}^{(i)} \hat{\phi}_j^{(i)} : 1 \leq i \leq m, 1 \leq j \leq L_i\} \\ &= \text{span}\{\Pi_{aux}^{(i)} \tilde{\phi}_j^{(i)} : 1 \leq i \leq m, 1 \leq j \leq L_i\} \\ &= \text{span}\{\psi_j^{(i)} : 1 \leq i \leq m, 1 \leq j \leq L_i\} \end{aligned}$$

that imply (cf. (4.10))

$$\dim(\text{span}\{\hat{\phi}_j^{(i)} - \mathfrak{C}_h \hat{\phi}_j^{(i)} : 1 \leq i \leq m, 1 \leq j \leq L_i\}) = \sum_{i=1}^m L_i = \dim V_{aux}^{\text{ms},h}.$$

□

5. A LOCALIZED MULTISCALE FINITE ELEMENT METHOD

We will use a special basis of $\text{Ker } \Pi_{aux}$ in the construction of the localized multiscale finite element space. Below $\mathbf{A} \in \mathbb{R}^{n \times n}$ is the symmetric positive definite stiffness matrix representing the bilinear form $a(\cdot, \cdot)$ with respect to the standard nodal basis functions of V_h , where $n = \dim V_h$.

5.1. The Modified Gram-Schmidt Algorithm. A set of vectors $\mathbf{w}_1, \dots, \mathbf{w}_q$ are \mathbf{A} -orthogonal if $\mathbf{w}_j^T \mathbf{A} \mathbf{w}_k = 0$ for $j \neq k$. They are \mathbf{A} -orthonormal if in addition they are \mathbf{A} -unit vectors, i.e., $\mathbf{w}_j^T \mathbf{A} \mathbf{w}_j = 1$ for $j = 1, \dots, q$.

Given linearly independent vectors $\mathbf{v}_1, \dots, \mathbf{v}_q \in \mathbb{R}^n$, the modified Gram-Schmidt algorithm (cf. Algorithm 5.1) overwrites $\mathbf{v}_1, \dots, \mathbf{v}_q$ so that the resulting vectors are \mathbf{A} -orthonormal and have the same span as the original $\mathbf{v}_1, \dots, \mathbf{v}_q$.

Algorithm 5.1 The modified Gram-Schmidt algorithm.

```

for  $i = 1$  to  $q$ 
   $r_{ii} = \sqrt{\mathbf{v}_i^T \mathbf{A} \mathbf{v}_i}$ 
   $\mathbf{v}_i \leftarrow \mathbf{v}_i / r_{ii}$ 
  for  $j = i + 1$  to  $q$ 
     $r_{ij} = \mathbf{v}_i^T \mathbf{A} \mathbf{v}_j$ 
     $\mathbf{v}_j \leftarrow \mathbf{v}_j - \mathbf{v}_i r_{ij}$ 
  end
end

```

Properties of the modified Gram-Schmidt algorithm can be found in [21].

5.2. Construction of the Special Basis Functions of $\text{Ker } \Pi_{aux}$. We apply a domain decomposition substructuring strategy to construct three types of basis vectors/functions according to the three types of functions $\tilde{\phi}_p$ in Remark 4.6.

5.2.1. Basis Vectors/Functions Associated with the Interior of an Element of \mathcal{T}_H . Let the functions $\phi_{p_1} - \tilde{\phi}_{p_1}, \dots, \phi_{p_{q_i}} - \tilde{\phi}_{p_{q_i}}$ be represented by the vectors $\mathbf{v}_1, \dots, \mathbf{v}_{q_i} \in \mathbb{R}^n$ with respect to the standard nodal basis of V_h , where p_1, \dots, p_{q_i} are the vertices of \mathcal{T}_h interior to $K_i \in \mathcal{T}_H$ and not a dual node (cf. Section 4.1). We apply the modified Gram-Schmidt algorithm in Section 5.1 to replace $\mathbf{v}_1, \dots, \mathbf{v}_{q_i}$ by a set of \mathbf{A} -orthonormal vectors. The corresponding finite element functions are supported on K_i , just like the original basis functions $\phi_{p_1} - \tilde{\phi}_{p_1}, \dots, \phi_{p_{q_i}} - \tilde{\phi}_{p_{q_i}}$.

Remark 5.1. The computational cost of this process is $O((n/m)^3)$ for each of the m elements of \mathcal{T}_H and these computations can be carried out in parallel.

5.2.2. Basis Vectors/Functions Associated with the Interior of an Edge of \mathcal{T}_H . Let E be an interior edge of \mathcal{T}_H shared by $K_1^E, K_2^E \in \mathcal{T}_H$. Given a vertex p of \mathcal{T}_h in the interior of E , we first replace the vector representing $\phi_p - \tilde{\phi}_p$ by a vector that is \mathbf{A} -orthogonal to the vectors constructed in Section 5.2.1 for the elements K_1^E and K_2^E . Then we apply the modified Gram-Schmidt algorithm in Section 5.1 to replace these vectors by n_E \mathbf{A} -orthonormal vectors, where n_E is the number of vertices of \mathcal{T}_h interior to E . The corresponding finite element functions are supported on $K_1^E \cup K_2^E$, just like the original basis functions.

Remark 5.2. The computational cost of this process is $O((n/m)^{5/2})$ for each of the $O(m)$ many interior edges of \mathcal{T}_H and these computations can be carried out in parallel.

5.2.3. Basis Vectors/Functions Associated with an Interior Vertex of \mathcal{T}_H . Let p be an interior vertex of \mathcal{T}_H that is the common vertex of the four elements K_1^p, \dots, K_4^p of \mathcal{T}_H and the four edges E_1^p, \dots, E_4^p of \mathcal{T}_H . We replace the vector representing $\phi_p - \tilde{\phi}_p$ by a \mathbf{A} -unit vector that is \mathbf{A} -orthogonal to the vectors constructed in Section 5.2.1 for K_1^p, \dots, K_4^p and the vectors constructed in Section 5.2.2 for E_1^p, \dots, E_4^p . The corresponding finite element function is supported on $K_1^p \cup K_2^p \cup K_3^p \cup K_4^p$, just like the original basis function $\phi_p - \tilde{\phi}_p$.

Remark 5.3. The computational cost of this process is $O((n/m)^2)$ for each of the $O(m)$ many interior vertices of \mathcal{T}_H and these computations can be carried out in parallel.

Remark 5.4. By construction each function $\phi_p - \tilde{\phi}_p$ (where p is not a dual node) is replaced by a normalized finite element function supported in the same elements from \mathcal{T}_H as $\phi_p - \tilde{\phi}_p$.

5.3. A Matrix Form of the Correction Equation (4.16). Let $\ell = n - L = \dim \text{Ker } \Pi_{aux}$ and $\mathbf{K} \in \mathbb{R}^{n \times \ell}$ be the matrix with full rank whose columns contain the basis vectors constructed in Section 5.2. We can then write the correction equation (4.16) as

$$\mathbf{K}^T \mathbf{A} \mathbf{K} \mathbf{x} = \mathbf{K}^T \mathbf{A} \mathbf{v},$$

where \mathbf{Kx} is the vector representing $\mathfrak{C}_h v$ with respect to the standard nodal basis of V_h and \mathbf{v} is the vector representing $v \in V_h$. By construction the matrix $\mathbf{K}^T \mathbf{A} \mathbf{K} \in \mathbb{R}^{\ell \times \ell}$ is symmetric positive definite.

Since all the columns of \mathbf{K} are \mathbf{A} -unit vectors by the construction in Section 5.2, the diagonal part of $\mathbf{K}^T \mathbf{A} \mathbf{K}$ is the identity matrix $\mathbf{I} \in \mathbb{R}^{\ell \times \ell}$, i.e.,

$$(5.1) \quad \mathbf{K}^T \mathbf{A} \mathbf{K} = \mathbf{I} + \mathbf{B},$$

where $\mathbf{B} \in \mathbb{R}^{\ell \times \ell}$ is a symmetric off-diagonal matrix. Moreover $\mathbf{B}(i, j) = 0$ except (i) $\mathbf{K}(:, i)$ is a basis vector associated with a vertex of \mathcal{T}_h interior to an edge E_i of \mathcal{T}_H constructed in Section 5.2.2, $\mathbf{K}(:, j)$ is a basis vector associated with a vertex of \mathcal{T}_h interior to another edge E_j of \mathcal{T}_H , and E_i and E_j are both edges of one of the elements in \mathcal{T}_H ; (ii) $\mathbf{K}(:, i)$ is a basis vector associated with an interior vertex p_i of \mathcal{T}_H constructed in Section 5.2.3, $\mathbf{K}(:, j)$ is a basis vector associated with another interior vertex p_j of \mathcal{T}_H , and p_i and p_j are endpoints of an edge E of \mathcal{T}_H . Therefore $\mathbf{K}^T \mathbf{A} \mathbf{K}$ is a sparse matrix because of (5.1).

We will denote the condition number of $\mathbf{K}^T \mathbf{A} \mathbf{K}$ by \mathfrak{K} , i.e,

$$(5.2) \quad \mathfrak{K} = \frac{\lambda_{\max}(\mathbf{K}^T \mathbf{A} \mathbf{K})}{\lambda_{\min}(\mathbf{K}^T \mathbf{A} \mathbf{K})}.$$

Remark 5.5. \mathfrak{K} can be estimated through conjugate gradient iterations.

Remark 5.6. Numerical results indicate that the condition number \mathfrak{K} is moderate even for large β and it decreases as H decreases. Heuristically we can treat $\mathbf{K}^T \mathbf{A} \mathbf{K}$ as a preconditioned matrix where the preconditioner is similar to a substructuring domain decomposition preconditioner (cf. [3]) where global communication is implied by the definition of $\text{Ker } \Pi_{aux}$.

5.4. A Localized Multiscale Finite Element Method. Let $\mathbf{f}_j^{(i)} \in \mathbb{R}^n$ ($1 \leq i \leq m, 1 \leq j \leq L_i$) be the vector that represents the normalized hat function $\hat{\phi}_j^{(i)}$ associated with the dual node $\hat{p}_j^{(i)}$ (cf. Section 4.1) with respect to the standard nodal basis of V_h . We apply k iterations of the conjugate gradient algorithm (cf. [9, 22]) with initial guess $\mathbf{0}$ to the corrector equation

$$(5.3) \quad \mathbf{K}^T \mathbf{A} \mathbf{K} \mathbf{x} = \mathbf{K}^T \mathbf{A} \mathbf{f}_j^{(i)}$$

to obtain an approximate solution $\hat{\mathbf{x}}_j^{(i)}$ and define $\mathfrak{C}_{h,k} \hat{\phi}_j^{(i)}$ to be the finite element function represented by $\mathbf{K} \hat{\mathbf{x}}_j^{(i)}$. We can then extend $\mathfrak{C}_{h,k}$ to be a linear operator from V_h^d to $\text{Ker } \Pi_{aux}$ by linearity.

Remark 5.7. We can regard $\mathbf{K} \hat{\mathbf{x}}_j$ as an approximate solution for $\mathfrak{C}_h v$ in (4.16) (with $v = \hat{\phi}_j^{(i)}$) obtained by a preconditioned conjugate gradient algorithm.

Remark 5.8. According to Remark 5.4, the function $\mathfrak{C}_{h,k} \hat{\phi}_j^{(i)}$ is supported on a domain obtained by adding roughly k layers of elements in \mathcal{T}_H to K_i , i.e., it is a localized correction of $\hat{\phi}_j^{(i)}$.

Let $V_{aux,k}^{\text{ms},h}$ be the space of functions spanned by $\hat{\phi}_j^{(i)} - \mathfrak{C}_{h,k} \hat{\phi}_j^{(i)}$ for $1 \leq i \leq m$ and $1 \leq j \leq L_i$. The localized multiscale finite element method for (1.1) is to find $u_{aux,k}^{\text{ms},h} \in V_{aux,k}^{\text{ms},h}$ such that

$$(5.4) \quad a(u_{aux,k}^{\text{ms},h}, v) = \int_{\Omega} f v \, dx \quad \forall v \in V_{aux,k}^{\text{ms},h}.$$

Remark 5.9. Since $\Pi_{aux}(\hat{\phi}_j^{(i)} - \mathfrak{C}_{h,k}\hat{\phi}_j^{(i)}) = \Pi_{aux}\hat{\phi}_j^{(i)}$, the functions $\hat{\phi}_j^{(i)} - \mathfrak{C}_{h,k}\hat{\phi}_j^{(i)}$ for $1 \leq i \leq m$ and $1 \leq j \leq L_i$ are linearly independent by Remark 4.4 and hence $\dim V_{aux,k}^{\text{ms,h}} = \dim V_{aux}^{\text{ms,h}}$.

Remark 5.10. The localized multiscale finite element method is a reduced order method. The time consuming construction of the basis of the space $V_{aux,k}^{\text{ms,h}}$ can be carried out in the off-line stage. The on-line solution of (5.4) is very fast when the dimension of $V_{aux,k}^{\text{ms,h}}$ is moderate.

6. ANALYSIS OF THE LOCALIZED MULTISCALE FINITE ELEMENT METHOD

It follows from (4.6), (4.16), (5.3) and the theory of the conjugate gradient algorithm (cf. [9, 22]) that

$$(6.1) \quad \|\mathfrak{C}_h\hat{\phi}_j^{(i)} - \mathfrak{C}_{h,k}\hat{\phi}_j^{(i)}\|_a \leq \frac{2q^k}{1+q^{2k}} \|\mathfrak{C}_h\hat{\phi}_j^{(i)}\|_a \leq \frac{2q^k}{1+q^{2k}} \|\hat{\phi}_j^{(i)}\|_a = \frac{2q^k}{1+q^{2k}},$$

where, in view of (5.2), we can take

$$(6.2) \quad q = \frac{\sqrt{\mathfrak{K}} - 1}{\sqrt{\mathfrak{K}} + 1}.$$

6.1. Estimate for $\|\mathfrak{C}_h - \mathfrak{C}_{h,k}\|_a$. Let $\|\mathfrak{C}_h - \mathfrak{C}_{h,k}\|_a$ be the norm induced by the energy norm for the operator $\mathfrak{C}_h - \mathfrak{C}_{h,k}$ that maps V_h^d to $\text{Ker } \Pi_{aux}$.

Lemma 6.1. *We have the estimate*

$$(6.3) \quad \|\mathfrak{C}_h - \mathfrak{C}_{h,k}\|_a \leq \frac{2q^k}{1+q^{2k}} \sqrt{L}.$$

Proof. It follows from (2.8), (4.8), (6.1) and the Cauchy-Schwarz inequality that

$$\begin{aligned} \|(\mathfrak{C}_h - \mathfrak{C}_{h,k}) \sum_{i=1}^m \sum_{j=1}^{L_i} c_j^{(i)} \hat{\phi}_j^{(i)}\|_a &\leq \sum_{i=1}^m \sum_{j=1}^{L_i} |c_j^{(i)}| \|(\mathfrak{C}_h - \mathfrak{C}_{h,k})\hat{\phi}_j^{(i)}\|_a \\ &\leq \frac{2q^k}{1+q^{2k}} \sum_{i=1}^m \sum_{j=1}^{L_i} |c_j^{(i)}| \\ &\leq \frac{2q^k}{1+q^{2k}} \left(\sum_{i=1}^m L_i \right)^{\frac{1}{2}} \left(\sum_{i=1}^m \sum_{j=1}^{L_i} |c_j^{(i)}|^2 \right)^{\frac{1}{2}} \\ &= \frac{2q^k}{1+q^{2k}} \sqrt{L} \left\| \sum_{i=1}^m \sum_{j=1}^{L_i} c_j^{(i)} \hat{\phi}_j^{(i)} \right\|_a, \end{aligned}$$

which implies (6.3). \square

6.2. Error Estimates for $u_{aux,k}^{\text{ms},h}$. We will denote by M the number $\max_{1 \leq i \leq m} M_i$, where M_i is defined in (4.13).

Theorem 6.2. *The solution $u_{aux,k}^{\text{ms},h}$ of (5.4) satisfies the estimate*

$$(6.4) \quad \|u_h - u_{aux,k}^{\text{ms},h}\|_a \leq \|u_h - u_{aux}^{\text{ms},h}\|_a + \frac{2q^k}{1+q^{2k}} \sqrt{L} \sqrt{M} H^{-1} \sqrt{\beta} \|f\|_{L^2(\Omega)},$$

where $u_h \in V_h$ (resp., $u_{aux}^{\text{ms},h}$) satisfies (1.3) (resp., (4.3)), and q is defined in (6.2).

Proof. Let $u_h^{(d)} \in V_h^d$ be defined by

$$(6.5) \quad u_h^{(d)} = \sum_{i=1}^m \sum_{j=1}^{L_i} s_i(u_h, \psi_j^{(i)}) \tilde{\phi}_j^{(i)}.$$

Then we have, in view of (3.1), (3.7) and (4.14),

$$\Pi_{aux} u_h^{(d)} = \Pi_{aux} u_h,$$

and hence $u_h - u_h^{(d)}$ belongs to $\text{Ker } \Pi_{aux}$ so that

$$(6.6) \quad \mathfrak{C}_h(u_h - u_h^{(d)}) = u_h - u_h^{(d)}.$$

Note that by construction (cf. Section 5.4)

$$(6.7) \quad u_h^{(d)} - \mathfrak{C}_{h,k} u_h^{(d)} \text{ belongs to } V_{aux,k}^{\text{ms},h}.$$

It follows from (4.17), (6.6), (6.7), the Galerkin orthogonality of the LOD multiscale finite element method and the triangle inequality that

$$(6.8) \quad \begin{aligned} \|u_h - u_{aux,k}^{\text{ms},h}\|_a &\leq \|u_h - (u_h^{(d)} - \mathfrak{C}_{h,k} u_h^{(d)})\|_a \\ &\leq \|\mathfrak{C}_h u_h\|_a + \|(\mathfrak{C}_h - \mathfrak{C}_{h,k}) u_h^{(d)}\|_a = \|u_h - u_{aux}^{\text{ms},h}\|_a + \|(\mathfrak{C}_h - \mathfrak{C}_{h,k}) u_h^{(d)}\|_a, \end{aligned}$$

and we have

$$(6.9) \quad \|(\mathfrak{C}_h - \mathfrak{C}_{h,k}) u_h^{(d)}\|_a \leq \frac{2q^k}{1+q^{2k}} \sqrt{L} \|u_h^{(d)}\|_a$$

by (6.3).

From (1.2), (1.4), (1.5), (2.4), (4.13) and (6.5) we find

$$\begin{aligned} \|u_h^{(d)}\|_a^2 &= \sum_{i=1}^m a \left(\sum_{j=1}^{L_i} s_i(u_h, \psi_j^{(i)}) \tilde{\phi}_j^{(i)}, \sum_{\ell=1}^{L_i} s_i(u_h, \psi_{\ell}^{(i)}) \tilde{\phi}_{\ell}^{(i)} \right) \\ &\leq \sum_{i=1}^m M_i \sum_{j=1}^{L_i} [s_i(u_h, \psi_j^{(i)})]^2 \\ &\leq M \sum_{i=1}^m \sum_{j=1}^{L_i} [s_i(u_h, \psi_j^{(i)})]^2 \\ &\leq M H^{-2} \|u_h\|_{L^2(\Omega; \kappa)}^2 \end{aligned}$$

$$\begin{aligned}
&\leq MH^{-2}\beta\|u_h\|_{L^2(\Omega)}^2 \\
&\leq MH^{-2}\beta\|u_h\|_a^2 \\
&\leq MH^{-2}\beta\|f\|_{L^2(\Omega)}^2,
\end{aligned}$$

and hence

$$(6.10) \quad \|u_h^{(d)}\|_a \leq \sqrt{M}H^{-1}\sqrt{\beta}\|f\|_{L^2(\Omega)}.$$

The estimate (6.4) follows from (6.8)–(6.10). \square

Putting Theorem 4.1 and Theorem 6.2 together, we arrive at the estimate

$$(6.11) \quad \|u_h - u_{aux,k}^{\text{ms},h}\|_a \leq \left[C_*H + \frac{2q^k}{1+q^{2k}}\sqrt{L}\sqrt{M}H^{-1}\sqrt{\beta} \right] \|f\|_{L^2(\Omega)},$$

where the constants L , C_* , M and q are available through the construction of $V_{aux}^{(i)}$, (3.4), (4.13), Remark 5.5, and (6.2).

It follows from (6.11) that

$$(6.12) \quad \|u_h - u_{aux,k}^{\text{ms},h}\|_a \leq (C_* + 1)H\|f\|_{L^2(\Omega)}$$

if k is sufficiently large so that

$$(6.13) \quad 2q^k\sqrt{L}\sqrt{M}\sqrt{\beta} \leq H^2.$$

A standard duality argument then yields

$$(6.14) \quad \|u_h - u_{aux,k}^{\text{ms},h}\|_{L^2(\Omega)} \leq [(C_* + 1)H]^2\|f\|_{L^2(\Omega)}.$$

Remark 6.3. The estimates (6.12) and (6.14) indicate that the performance of the localized multiscale finite element method is similar to the performance of standard finite element methods for the homogeneous Dirichlet boundary value problem for the Poisson equation on smooth or convex domains.

7. NUMERICAL RESULTS

The domain Ω in the numerical examples is the unit square $(0, 1) \times (0, 1)$ and the function $f(x)$ in all the examples is defined by

$$(7.1) \quad f(x) = \begin{cases} 0 & \text{for } x \in [0, \frac{1}{2}) \times [0, 1] \\ 1 & \text{for } x \in [\frac{1}{2}, 1] \times [0, 1] \end{cases}$$

and $\|f\|_{L^2(\Omega)} = 1/2$.

For each example we obtain the following data from the computation:

- The number \sqrt{L} , where $L = \sum_{i=1}^m L_i$ and L_i is the number of eigenfunctions in the local auxiliary space $V_{aux}^{(i)}$ (cf. Section 2).
- The number \sqrt{M} , where $M = \max_{1 \leq i \leq m} M_i$ and M_i is defined in (4.13).
- The contraction number q of the conjugate gradient iteration defined in (6.2).

- The smallest integer k that satisfies (6.13).

Then we construct the basis functions of the localized multiscale finite element space $V_{aux,k}^{\text{ms},h}$ (cf. Section 5.1–Section 5.3). Finally for each K_i we run the modified Gram-Schmidt algorithm (Algorithm 5.1) for the basis functions of $V_{aux,k}^{\text{ms},h}$ that are associated with the dual nodes in each K_i , which generates a new set of basis functions of $V_{aux,k}^{\text{ms},h}$. All these can be carried out in the off-line stage.

In the on-line stage, the equation (5.4) is solved by using the basis of $V_{aux,k}^{\text{ms},h}$ generated at the end of the off-line stage. The solution by the backslash command in MATLAB is very fast (cf. Table 7.4, Table 7.7 and Table 7.11).

The computations were carried out on a Dell Inspiron 13 Laptop (11th Gen Intel(R) Core(TM) i5-11320H @ 3.20GHz (2.50 GHz), RAM: 8.00GB). The conjugate gradient iteration used a tolerance of 10^{-14} for the relative error as the stopping criterion.

Example 7.1. This is the example from [20, Section 5.2] with four high contrast channels in the unit square (cf. Figure 7.1).

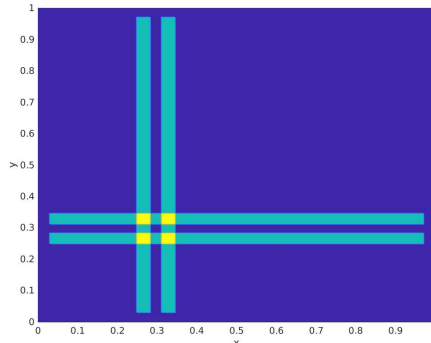


FIGURE 7.1. Four high contrast channels.

The diffusion coefficient $\kappa(x)$ is defined by

$$\kappa(x) = A(x_1, x_2) + A(x_2, x_1),$$

where

$$A(x) = \begin{cases} \beta/2 & \text{for } x \in [\frac{8}{32}, \frac{9}{32}] \times [\frac{1}{32}, \frac{31}{32}] \cup [\frac{10}{32}, \frac{11}{32}] \times [\frac{1}{32}, \frac{31}{32}] \\ 1 & \text{elsewhere} \end{cases}.$$

We solve the boundary value problem (1.1) for $\beta = 10^2, 10^4, 10^6$ and 10^8 . We take $h = 1/256$ and $H = 1/8, 1/16, 1/32, 1/64$. The data generated by the computation are displayed in Table 7.1.

The estimates for the energy error and L^2 error according to (6.12) and (6.14) are shown in Table 7.2, and the actual energy errors and L^2 errors can be found in Table 7.3. It is observed that for a given H , the actual errors are independent of the contrast β . By comparing these two tables we see that the estimates (6.12) and (6.14) are satisfied.

| $H \setminus \beta$ | 10^2 | | | | 10^4 | | | | 10^6 | | | | 10^8 | | | |
|---------------------|------------|-------------------|------|-----|------------|-------------------|------|-----|------------|-------------------|------|-----|------------|-------------------|------|-----|
| | \sqrt{L} | \sqrt{M} | q | k |
| 1/8 | 8.6 | 2.1×10^6 | 0.54 | 39 | 8.6 | 1.6×10^5 | 0.56 | 41 | 8.6 | 9.9×10^5 | 0.56 | 48 | 8.6 | 1.0×10^7 | 0.56 | 56 |
| 1/16 | 16 | 4.2×10^3 | 0.44 | 24 | 24 | 4.2×10^4 | 0.44 | 30 | 16 | 4.1×10^5 | 0.44 | 36 | 16 | 4.1×10^6 | 0.44 | 42 |
| 1/32 | 32 | 2.5×10^2 | 0.40 | 21 | 32 | 2.5×10^2 | 0.40 | 24 | 32 | 2.5×10^2 | 0.40 | 26 | 32 | 2.5×10^2 | 0.40 | 29 |
| 1/64 | 64 | 5.0×10^1 | 0.38 | 21 | 64 | 5.0×10^1 | 0.38 | 23 | 64 | 5.0×10^1 | 0.38 | 26 | 64 | 5.0×10^1 | 0.38 | 28 |

TABLE 7.1. Data generated by the computation for Example 7.1.

| H | $\frac{1}{8}$ | $\frac{1}{16}$ | $\frac{1}{32}$ | $\frac{1}{64}$ |
|-----------------------|----------------------|----------------------|----------------------|----------------------|
| Energy Error Estimate | 1.2×10^{-1} | 5.9×10^{-2} | 3.0×10^{-2} | 1.5×10^{-2} |
| L^2 Error Estimate | 1.4×10^{-2} | 3.5×10^{-3} | 8.8×10^{-4} | 2.2×10^{-4} |

TABLE 7.2. Estimates (6.12) and (6.14) for Example 7.1.

| $H \setminus \beta$ | 10^2 | | 10^4 | | 10^6 | | 10^8 | |
|---------------------|----------------------|----------------------|----------------------|----------------------|----------------------|----------------------|----------------------|----------------------|
| | Energy Error | L^2 Error |
| 1/8 | 3.1×10^{-3} | 4.8×10^{-5} |
| 1/16 | 1.7×10^{-3} | 1.6×10^{-5} |
| 1/32 | 3.5×10^{-4} | 1.5×10^{-6} |
| 1/64 | 1.1×10^{-4} | 2.3×10^{-7} |

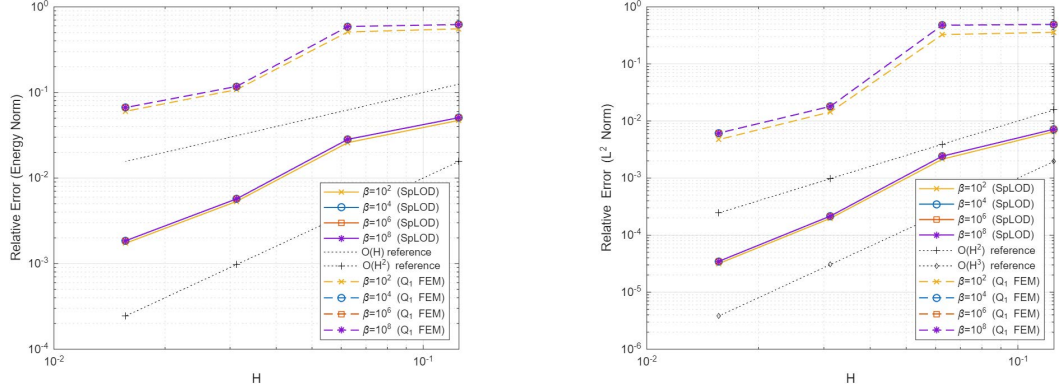
TABLE 7.3. Energy and L^2 errors for Example 7.1.

The convergence histories in the energy norm and the L^2 norm for the standard Q_1 finite element method and the localized multiscale finite element method are displayed in Figure 7.2. The advantage of the multiscale finite element method is clearly observed. The order of convergence of the multiscale finite element method in the energy norm is between 1 and 2, and the order of convergence in the L^2 norm is between 2 and 3. The relative errors of our method also appear to be smaller than the ones in [20].

Finally we report in Table 7.4 the solution times of (5.4) by the backslash command in MATLAB.

| $H \setminus \beta$ | 10^2 | 10^4 | 10^6 | 10^8 |
|---------------------|-----------------------|-----------------------|-----------------------|-----------------------|
| 1/8 | 7.83×10^{-5} | 6.95×10^{-5} | 7.95×10^{-5} | 1.10×10^{-4} |
| 1/16 | 9.33×10^{-4} | 7.69×10^{-4} | 1.08×10^{-3} | 9.39×10^{-4} |
| 1/32 | 2.13×10^{-2} | 2.14×10^{-2} | 2.11×10^{-2} | 1.98×10^{-2} |

TABLE 7.4. Solution times (in seconds) of (5.4) by the backslash command in MATLAB for Example 7.1.

FIGURE 7.2. Relative energy errors (left) and relative L^2 errors (right) for Example 7.1.

Example 7.2. This is an example of irregular channels in the unit square where the diffusion coefficient $\kappa(x) = \beta$ in the red region and 1 elsewhere (cf. Figure 7.3).

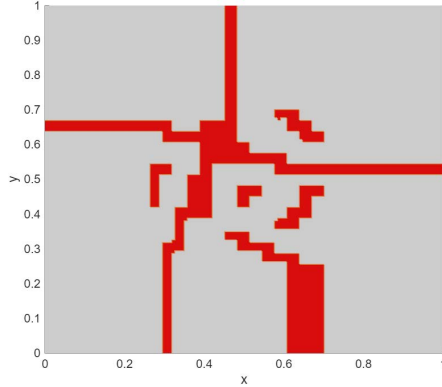


FIGURE 7.3. Irregular high contrast channels.

We solve the boundary value problem (1.1) for $\beta = 10^2, 10^4, 10^6$ and 10^8 . We take $h = 1/256$ and $H = 1/8, 1/16, 1/32, 1/64$. The data generated by the computation are displayed in Table 7.5.

| H | β | 10 ² | | | | 10 ⁴ | | | | 10 ⁶ | | | | 10 ⁸ | | | |
|------|---------|-----------------|-------------------|------|-----|-----------------|-------------------|------|-----|-----------------|-------------------|------|-----|-----------------|-------------------|------|-----|
| | | \sqrt{L} | \sqrt{M} | q | k |
| 1/8 | 10^2 | 8.7 | 3.9×10^5 | 0.46 | 29 | 8.7 | 2.3×10^6 | 0.46 | 34 | 8.7 | 2.3×10^7 | 0.46 | 40 | 8.7 | 2.3×10^8 | 0.46 | 46 |
| 1/16 | 10^2 | 17 | 1.5×10^5 | 0.47 | 31 | 17 | 1.5×10^5 | 0.47 | 34 | 17 | 6.6×10^5 | 0.47 | 39 | 17 | 6.6×10^6 | 0.47 | 46 |
| 1/32 | 10^2 | 32 | 1.3×10^4 | 0.41 | 26 | 32 | 2.6×10^4 | 0.41 | 29 | 32 | 1.4×10^5 | 0.41 | 34 | 32 | 1.4×10^6 | 0.41 | 39 |
| 1/64 | 10^2 | 64 | 1.9×10^2 | 0.41 | 24 | 64 | 1.8×10^3 | 0.42 | 29 | 64 | 1.8×10^4 | 0.42 | 35 | 64 | 1.8×10^5 | 0.42 | 40 |

TABLE 7.5. Data generated by the computation for Example 7.2.

The estimates for the energy error and L^2 error according to (6.12) and (6.14) are identical to the ones in Table 7.2, and the actual energy errors and L^2 errors can be found in Table 7.6.

The behavior of the errors are similar to that in Example 7.1, namely for a given H the errors are independent of the contrast β and the estimates (6.12) and (6.14) are satisfied.

| H | β | 10 ² | | 10 ⁴ | | 10 ⁶ | | 10 ⁸ | |
|------|---------|----------------------|----------------------|----------------------|----------------------|----------------------|----------------------|----------------------|----------------------|
| | | Energy Error | L^2 Error |
| 1/8 | | 8.6×10^{-3} | 2.4×10^{-4} | 8.9×10^{-3} | 2.6×10^{-4} | 8.9×10^{-3} | 2.6×10^{-4} | 8.9×10^{-3} | 2.6×10^{-4} |
| 1/16 | | 2.7×10^{-3} | 3.6×10^{-5} | 2.8×10^{-3} | 3.8×10^{-5} | 2.8×10^{-3} | 3.8×10^{-5} | 2.8×10^{-3} | 3.8×10^{-5} |
| 1/32 | | 1.5×10^{-3} | 1.1×10^{-5} | 1.5×10^{-3} | 1.2×10^{-5} | 1.5×10^{-3} | 1.2×10^{-5} | 1.5×10^{-3} | 1.2×10^{-5} |
| 1/64 | | 1.9×10^{-4} | 6.3×10^{-7} | 1.9×10^{-4} | 6.4×10^{-7} | 1.9×10^{-4} | 6.4×10^{-7} | 1.9×10^{-4} | 6.4×10^{-7} |

TABLE 7.6. Energy and L^2 errors for Example 7.2.

The convergence histories in the energy norm and the L^2 norm for the standard Q_1 finite element method and the localized multiscale finite element method are displayed in Figure 7.4. Again we observe the advantage of the multiscale finite element method over the standard Q_1 finite element method and the order of convergence of the multiscale finite element method in the energy (resp., L^2) norm is between 1 and 2 (resp., 2 and 3).

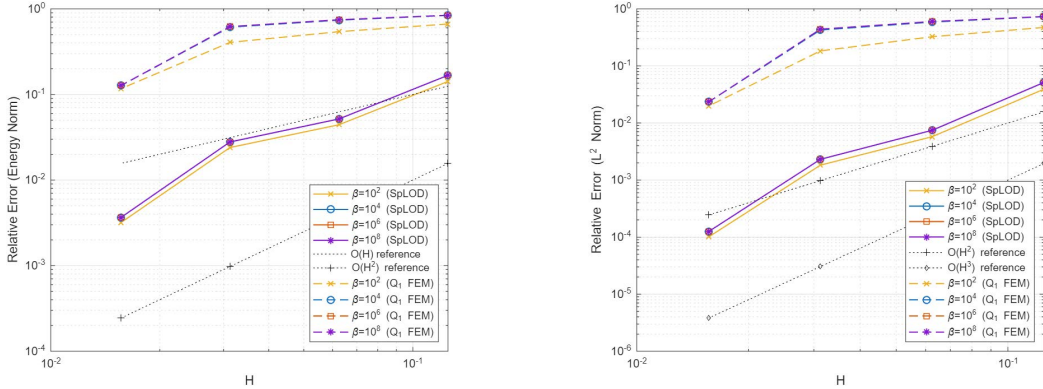


FIGURE 7.4. Relative energy errors (left) and relative L^2 errors (right) for Example 7.2.

The solution times of (5.4) by the backslash command in MATLAB are reported in Table 7.7.

| $H \setminus \beta$ | 10 ² | 10 ⁴ | 10 ⁶ | 10 ⁸ |
|---------------------|-----------------------|-----------------------|-----------------------|-----------------------|
| 1/8 | 8.78×10^{-5} | 7.47×10^{-5} | 7.64×10^{-5} | 7.91×10^{-5} |
| 1/16 | 1.77×10^{-3} | 1.53×10^{-3} | 1.45×10^{-3} | 1.68×10^{-3} |
| 1/32 | 2.86×10^{-2} | 2.52×10^{-2} | 2.28×10^{-2} | 2.43×10^{-2} |

TABLE 7.7. Solution times (in seconds) of (5.4) by the backslash command in MATLAB for Example 7.2.

Example 7.3. The picture in this example depicts a real-life geographical fracture found at www.beg.utexas.edu/eichhubl/Pages/Fracturemechanics.html, where the diffusion coefficient $\kappa(x) = \beta$ in the black region and 1 elsewhere (cf. Figure 7.5).

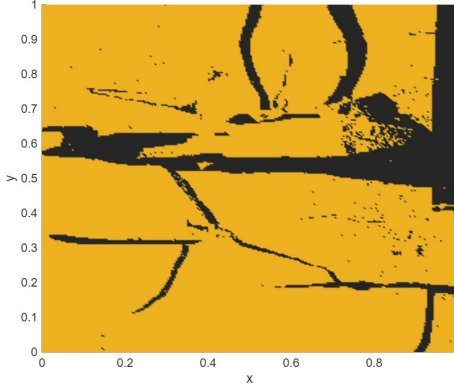


FIGURE 7.5. High contrast geographical fracture.

We solve the boundary value problem (1.1) for $\beta = 10^2, 10^4, 10^6$ and 10^8 . We take $h = 1/272$ and $H = 1/17, 1/34, 1/68$. The data generated by the computation are displayed in Table 7.8.

| $H \setminus \beta$ | 10^2 | | | | 10^4 | | | | 10^6 | | | | 10^8 | | | |
|---------------------|------------|-------------------|------|-----|------------|-------------------|------|-----|------------|-------------------|------|-----|------------|----------------------|------|-----|
| | \sqrt{L} | \sqrt{M} | q | k | \sqrt{L} | \sqrt{M} | q | k | \sqrt{L} | \sqrt{M} | q | k | \sqrt{L} | \sqrt{M} | q | k |
| 1/17 | 21 | 3.0×10^5 | 0.51 | 45 | 22 | 9.7×10^6 | 0.79 | 129 | 22 | 9.7×10^8 | 0.80 | 164 | 22 | 9.7×10^{10} | 0.80 | 195 |
| 1/34 | 38 | 2.9×10^4 | 0.41 | 27 | 38 | 2.0×10^5 | 0.41 | 32 | 38 | 8.3×10^6 | 0.41 | 39 | 38 | 5.0×10^8 | 0.41 | 46 |
| 1/68 | 71 | 1.0×10^4 | 0.44 | 31 | 71 | 2.0×10^4 | 0.45 | 35 | 71 | 1.1×10^5 | 0.45 | 40 | 71 | 1.1×10^6 | 0.45 | 46 |

TABLE 7.8. Data generated by the computation for Example 7.3.

The estimates for the energy error and L^2 error according to (6.12) and (6.14) are shown in Table 7.9, and the actual energy errors and L^2 errors can be found in Table 7.10. It is observed that for a given H the errors are independent of the contrast β and the estimates (6.12) and (6.14) are satisfied.

| H | $\frac{1}{7}$ | $\frac{1}{34}$ | $\frac{1}{68}$ |
|-----------------------|----------------------|----------------------|----------------------|
| Energy Error Estimate | 8.5×10^{-2} | 4.3×10^{-2} | 2.1×10^{-2} |
| L^2 Error Estimate | 7.3×10^{-3} | 1.9×10^{-3} | 4.5×10^{-4} |

TABLE 7.9. Estimates (6.12) and (6.14) for Example 7.3.

| $H \setminus \beta$ | 10^2 | | 10^4 | | 10^6 | | 10^8 | |
|---------------------|----------------------|----------------------|----------------------|----------------------|----------------------|----------------------|----------------------|----------------------|
| | Energy Error | L^2 Error |
| 1/17 | 4.1×10^{-3} | 5.1×10^{-5} | 4.2×10^{-3} | 5.8×10^{-5} | 4.2×10^{-3} | 5.9×10^{-5} | 4.2×10^{-3} | 5.8×10^{-5} |
| 1/34 | 1.5×10^{-3} | 1.0×10^{-5} | 1.4×10^{-3} | 1.0×10^{-5} | 1.4×10^{-3} | 1.0×10^{-5} | 1.4×10^{-3} | 1.0×10^{-5} |
| 1/68 | 4.5×10^{-4} | 1.5×10^{-6} | 4.6×10^{-4} | 1.6×10^{-6} | 4.6×10^{-4} | 1.6×10^{-6} | 4.6×10^{-4} | 1.6×10^{-6} |

TABLE 7.10. Energy and L^2 errors for Example 7.3.

The convergence histories in the energy norm and the L^2 norm for the standard Q_1 finite element method and the localized multiscale finite element method are displayed in Figure 7.6. Their behaviors are similar to those in Example 7.1 and Example 7.2.

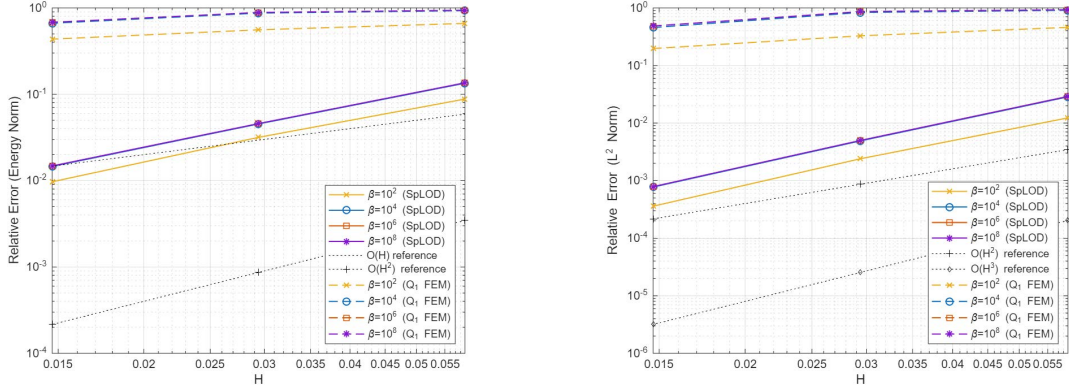


FIGURE 7.6. Relative energy errors (left) and relative L^2 errors (right) for Example 7.3.

Table 7.11 contains the solution times of (5.4) by the backslash command in MATLAB.

| $H \setminus \beta$ | 10^2 | 10^4 | 10^6 | 10^8 |
|---------------------|-----------------------|-----------------------|-----------------------|-----------------------|
| $1/17$ | 4.95×10^{-3} | 6.48×10^{-3} | 6.69×10^{-3} | 7.46×10^{-3} |
| $1/34$ | 4.82×10^{-2} | 5.22×10^{-2} | 4.71×10^{-2} | 4.60×10^{-2} |

TABLE 7.11. Solution times (in seconds) of (5.4) by the backslash command in MATLAB for Example 7.3.

8. CONCLUDING REMARKS

We have developed a multiscale finite element method for a model diffusion problem with rough and high contrast coefficients whose performance is similar to the performance of standard finite element methods for the Poisson equation on smooth or convex domains. We established simple explicit error estimates under conditions that can be verified from the outputs of the computation in the construction of the multiscale finite element space.

The method was presented for the unit square for clarity. However, since the construction and analysis of our method are based purely on techniques in numerical linear algebra, the extension to arbitrary domains in two and three dimensions with simplicial triangulations and the P_1 finite element is straightforward.

It would be interesting to carry out an analysis of the condition number of the matrix $\mathbf{K}^T \mathbf{A} \mathbf{K}$ in Section 5.3 based on domain decomposition techniques (cf. Remark 5.6).

APPENDIX A. LOWER BOUNDS FOR THE EIGENVALUE μ_i

We will derive the lower bounds of the eigenvalues stated in Remark 2.1.

A.1. Let K_i be one of the (closed) elements of \mathcal{T}_H that is disjoint from $\partial\Omega$. By scaling, the eigenvalue problem (2.1)–(2.2) with $\kappa = 1$ is equivalent to the following discrete eigenvalue problem on the unit square Ω : Find $\mu_j > 0$ such that

$$(A.1) \quad \int_{\Omega} \nabla \psi_j \cdot \nabla w \, dx = \mu_j \int_{\Omega} \psi_j w \, dx \quad \forall w \in V_{h/H},$$

$$(A.2) \quad \int_{\Omega} \psi_j^2 \, dx = 1,$$

where $V_{h/H}$ is the Q_1 finite element subspace of $H^1(\Omega)$ associated with a uniform triangulation of Ω by squares whose edges have length h/H .

Observe that the discrete eigenvalue problem (A.1)–(A.2) is a finite element approximation of the following continuous eigenvalue problem: Find $\hat{\mu}_j > 0$ such that

$$(A.3) \quad \int_{\Omega} \nabla \hat{\psi}_j \cdot \nabla w \, dx = \hat{\mu}_j \int_{\Omega} \hat{\psi}_j w \, dx \quad \forall w \in H^1(\Omega),$$

$$(A.4) \quad \int_{\Omega} \hat{\psi}_j^2 \, dx = 1.$$

The smallest eigenvalue for (A.3)–(A.4) is given by $\hat{\mu}_1 = \pi^2$ with eigenfunction $\hat{\psi}_1(x) = \cos(\pi x_1)$. It is characterized by

$$(A.5) \quad \hat{\mu}_1 = \min_{\substack{w \in H^1(\Omega), \|w\|_{L^2(\Omega)}=1 \\ \int_{\Omega} w \, dx=0}} \int_{\Omega} |\nabla w|^2 \, dx.$$

On the other hand the smallest eigenvalue μ_1 of (A.1)–(A.2) is characterized by

$$(A.6) \quad \mu_1 = \min_{\substack{w \in V_{h/H}, \|w\|_{L^2(\Omega)}=1 \\ \int_{\Omega} w \, dx=0}} \int_{\Omega} |\nabla w|^2 \, dx.$$

Comparing (A.5) and (A.6), we see that

$$(A.7) \quad \mu_1 \geq \hat{\mu}_1 = \pi^2.$$

A.2. Let K_i be one of the (closed) elements of \mathcal{T}_H that has only one edge on $\partial\Omega$. In this case the corresponding continuous eigenvalue problem is to find $\hat{\mu}_j$ such that

$$(A.8) \quad \int_{\Omega} \nabla \hat{\psi}_j \cdot \nabla w \, dx = \hat{\mu}_j \int_{\Omega} \hat{\psi}_j w \, dx \quad \forall w \in H^1(\Omega), w(0, t) = 0, 0 < t < 1,$$

$$(A.9) \quad \int_{\Omega} \hat{\psi}_j^2 \, dx = 1.$$

The smallest eigenvalue for (A.8)–(A.9) is $\hat{\mu}_1 = (\pi/2)^2$ with eigenfunction $\hat{\psi}_1(x) = \sin((\pi/2)x_1)$. It is characterized by

$$\hat{\mu}_1 = \min_{\substack{w \in H^1(\Omega), \|w\|_{L^2(\Omega)}=1 \\ w(0,t)=0, 0 < t < 1}} \int_{\Omega} |\nabla w|^2 \, dx$$

and hence provides a lower bound for the discrete eigenvalue characterized by

$$\mu_1 = \min_{\substack{w \in V_{h/H}, \|w\|_{L^2(\Omega)}=1 \\ w(0,t)=0, 0 < t < 1}} \int_{\Omega} |\nabla w|^2 dx.$$

A.3. Let K_i be one of the (closed) elements of \mathcal{T}_H that has two edges on $\partial\Omega$. In this case the corresponding continuous eigenvalue problem is to find $\hat{\mu}_j$ such that

$$(A.10) \quad \int_{\Omega} \nabla \hat{\psi}_j \cdot \nabla w dx = \hat{\mu}_j \int_{\Omega} \hat{\psi}_j w dx \quad \forall w \in H^1(\Omega), w(0, t) = w(t, 0) = 0, 0 < t < 1,$$

$$(A.11) \quad \int_{\Omega} \hat{\psi}_j^2 dx = 1.$$

The smallest eigenvalue for (A.8)–(A.9) is $\hat{\mu}_1 = \pi^2/2$ with eigenfunction

$$\hat{\psi}_1(x) = \sin((\pi/2)x_1) \sin((\pi/2)x_2).$$

It is characterized by

$$\hat{\mu}_1 = \min_{\substack{w \in H^1(\Omega), \|w\|_{L^2(\Omega)}=1 \\ w(0,t)=w(t,0)=0, 0 < t < 1}} \int_{\Omega} |\nabla w|^2 dx$$

and hence provides a lower bound for the discrete eigenvalue characterized by

$$\mu_1 = \min_{\substack{w \in V_{h/H}, \|w\|_{L^2(\Omega)}=1 \\ w(0,t)=w(t,0)=0, 0 < t < 1}} \int_{\Omega} |\nabla w|^2 dx.$$

REFERENCES

- [1] R.A. Adams and J.J.F. Fournier. *Sobolev Spaces (Second Edition)*. Academic Press, Amsterdam, 2003.
- [2] I. Babuška and R. Lipton. Optimal local approximation spaces for generalized finite element methods with application to multiscale problems. *Multiscale Model. Simul.*, 9:373–406, 2011.
- [3] J.H. Bramble, J.E. Pasciak, and A.H. Schatz. The construction of preconditioners for elliptic problems by substructuring, I. *Math. Comp.*, 47:103–134, 1986.
- [4] S.C. Brenner and L.R. Scott. *The Mathematical Theory of Finite Element Methods (Third Edition)*. Springer-Verlag, New York, 2008.
- [5] E.T. Chung, Y. Efendiev, and W.T. Leung. Constraint energy minimizing generalized multiscale finite element method. *Comput. Methods Appl. Mech. Engrg.*, 339:298–319, 2018.
- [6] P.G. Ciarlet. *The Finite Element Method for Elliptic Problems*. North-Holland, Amsterdam, 1978.
- [7] J. Galvis and Y. Efendiev. Domain decomposition preconditioners for multiscale flows in high-contrast media. *Multiscale Model. Simul.*, 8:1461–1483, 2010.
- [8] J. Galvis and Y. Efendiev. Domain decomposition preconditioners for multiscale flows in high contrast media: reduced dimension coarse spaces. *Multiscale Model. Simul.*, 8:1621–1644, 2010.
- [9] A. Greenbaum. *Iterative Methods for Solving Linear Systems*. SIAM, Philadelphia, 1997.
- [10] P.R. Halmos. *Finite Dimensional Vector Spaces*. Princeton University Press, Princeton, NJ, 1942.
- [11] P. Henning and D. Peterseim. Oversampling for the multiscale finite element method. *Multiscale Model. Simul.*, 11:1149–1175, 2013.
- [12] H.H. Kim and E.T. Chung. A BDDC algorithm with enriched coarse spaces for two-dimensional elliptic problems with oscillatory and high contrast coefficients. *Multiscale Model. Simul.*, 13:571–593, 2015.
- [13] C. Ma and R. Scheichl. Error estimates for discrete generalized FEMs with locally optimal spectral approximations. *Math. Comp.*, 91:2539–2569, 2022.

- [14] C. Ma, R. Scheichl, and T. Dodwell. Novel design and analysis of generalized finite element methods based on locally optimal spectral approximations. *SIAM J. Numer. Anal.*, 60:244–273, 2022.
- [15] A. Målqvist and D. Peterseim. Localization of elliptic multiscale problems. *Math. Comp.*, 83:2583–2603, 2014.
- [16] A. Målqvist and D. Peterseim. *Numerical Homogenization by Localized Orthogonal Decomposition*. SIAM, Philadelphia, 2021.
- [17] A.L. Madureira and M. Sarkis. Hybrid localized spectral decomposition for multiscale problems. *SIAM J. Numer. Anal.*, 59:829–863, 2021.
- [18] A.L. Madureira and M. Sarkis. Spectral ACMS: a robust localized approximated component mode synthesis method. *SIAM J. Numer. Anal.*, 63:1055–1077, 2025.
- [19] R. Maier. A high-order approach to elliptic multiscale problems with general unstructured coefficients. *SIAM J. Numer. Anal.*, 59:1067–1089, 2021.
- [20] D. Peterseim and R. Scheichl. Robust numerical upscaling of elliptic multiscale problems at high contrast. *Comput. Methods Appl. Math.*, 16:579–603, 2016.
- [21] M. Rozložník, M. Tůma, A. Smoktunowicz, and J. Kopal. Numerical stability of orthogonalization methods with a non-standard inner product. *BIT*, 52:1035–1058, 2012.
- [22] Y. Saad. *Iterative Methods for Sparse Linear Systems*. SIAM, Philadelphia, 2003.
- [23] N. Spillane, V. Dolean, P. Hauret, F. Nataf, C. Pechstein, and R. Scheichl. Abstract robust coarse spaces for systems of PDEs via generalized eigenproblems in the overlaps. *Numer. Math.*, 126:741–770, 2014.

SUSANNE C. BRENNER, DEPARTMENT OF MATHEMATICS AND CENTER FOR COMPUTATION AND TECHNOLOGY, LOUISIANA STATE UNIVERSITY, BATON ROUGE, LA 70803, USA

Email address: brenner@math.lsu.edu

JOSÉ C. GARAY, INSTITUTE OF MATHEMATICS, AUGSBURG UNIVERSITY, AUGSBURG, GERMANY
Email address: jocgafer@gmail.com

LI-YENG SUNG, DEPARTMENT OF MATHEMATICS AND CENTER FOR COMPUTATION AND TECHNOLOGY, LOUISIANA STATE UNIVERSITY, BATON ROUGE, LA 70803, USA

Email address: sung@math.lsu.edu